Colloids and Surfaces B: Biointerfaces 192 (2020) 111047

Contents lists available at ScienceDirect

Colloids and Surfaces B: Biointerfaces

journal homepage: www.elsevier.com/locate/colsurfb

Protocols

The role of flow in bacterial biofilm morphology and wetting properties

Federica Recupido[a,b], Giuseppe Toscano[b], Rosarita Tatè[c], Maria Petala[d], Sergio Caserta[b,e,*], Thodoris D. Karapantsios[a,**], Stefano Guido[b,e]

[a] Division of Chemical Technology, School of Chemistry, Aristotle University of Thessaloniki, University Box 116, 54124, Thessaloniki, Greece
[b] Department of Chemical, Materials and Industrial Production Engineering (DICMaPI), University of Naples, Federico II, Piazzale V. Tecchio 80, 80125, Naples, Italy
[c] Institute of Genetics and Biophysics: "A. Buzzati-Traverso" (IGB-CNR), Pietro Castellino 111, 80131, Naples, Italy
[d] Department of Civil Engineering, Aristotle University of Thessaloniki, 54124 Thessaloniki, Greece
[e] CEINGE, Advanced Biotechnologies, 80145, Naples, Italy

ARTICLE INFO

Keywords:
Biofilm
Flow-induced-morphology
Confocal laser scanning microscopy
Wetting
Image analysis
Transport phenomena

ABSTRACT

Biofilms are bacterial communities embedded in an extracellular matrix, able to adhere to surfaces. Different experimental set-ups are widely used for *in vitro* biofilm cultivation; however, a well-defined comparison among different culture conditions, especially suited to interfacial characterization, is still lacking in the literature. The main objective of this work is to study the role of flow on biofilm formation, morphology and interfacial properties. Three different *in vitro* setups, corresponding to stagnant, shaking, and laminar flow conditions (custom-made flow cell), are used in this work to grow single strain biofilms of *Pseudomonas fluorescens* AR 11 on glass coupons.

Results show that flow conditions significantly influenced biofilm formation kinetics, affecting mass transfer and cell attachment/detachment processes. Distinct morphological patterns are found under different flow regimes. Static contact angle data do not depend significantly on biofilm growth conditions in the parametric range investigated in this work.

1. Introduction

Biofilms are surface-associated bacterial communities embedded in an extracellular matrix [1,2]. They represent a very common way of living of microorganisms in the natural environment because such communities give to their members several benefits, such as mechanical resistance, protection from antibiotics and cleaning solutions, adaptation to nutrient deficient conditions and capability to survive at changes in humidity [3,4]. A typical biofilm structure is made of about 10 % by weight of microorganisms, embedded in an aqueous matrix, mostly made of polysaccharides, accounting for the remaining 90 % by weight (on dry basis). From a morphological point of view, biofilms are complex systems, made of microbial layers and clusters, micro-channels, and voids, not necessarily uniformly distributed in space, and variable over time [5].

Negative implications of biofilms are substantial in many industrial processes and in health-related fields as well [6]. Probably the most adverse effect of biofilms is that biofilm can contaminate surfaces of vessels, pipes, fittings and vanes. Apart from altering the hygienic properties of these surfaces, the occasional detachment of biofilms (streamers) represents a hazard for process liquids affecting their cleanliness, sanitation and can even clog their flow [7]. On the other hand, there are also important positive implications of biofilms. As such, biofilms are used to enhance biotechnological processes such as bioremediation [8], wastewater treatment [9], and synthesis of fine chemicals [10] and biofuels [11] as well.

In many applications, biofilm formation process is strongly affected by flow conditions, where hydrodynamic forces are involved. Flow is relevant to several of the aforementioned steps, including attachment of planktonic cells to surfaces, detachment of cells from biofilm [12–15] and disposal of metabolites, delivery of nutrients and oxygen into biofilms, production of EPS and metabolic/genetic behaviours of biofilms [16] and bacterial quorum sensing [17].

Nowadays, a wide set of possible biofilms cultivation protocols are available from the literature. Typically, static laboratory set-ups, like multi-well plates, are broadly used in biofilm studies for their simplicity and for the possibility to investigate a variety of biofilm formation conditions, as regards the effect of medium composition. Examples of such experimental platforms are the Calgary device and the Biofilms ring test [18]. However, they are not able to reproduce realistic

* Corresponding author at: Department of Chemical, Materials and Industrial Production Engineering University of Naples, Federico II 80, 80125, Naples, Italy.
** Corresponding author at: Division of Chemical Technology, School of Chemistry, Aristotle University of Thessaloniki, 541 24, Thessaloniki, Greece.
E-mail addresses: sergio.caserta@unina.it (S. Caserta), karapant@chem.auth.gr (T.D. Karapantsios).

https://doi.org/10.1016/j.colsurfb.2020.111047
Received 4 December 2019; Received in revised form 26 March 2020; Accepted 11 April 2020
Available online 18 April 2020

Table 1
Process and geometrical parameters for the three *in vitro* conditions.

Type of Flow	Medium Volume / flow rate (mL / mL/min)	*P. fluorescens* inoculum volume (mL)	Surface area of glass coupon (cm^2)	Ratio of active surface area / total liquid volume (S/V) (cm^{-1})
Stagnant fluid	2	0.2	6.5	8.5
Shaken vessels	20	2	39.5	6.7
Shear flow, 0.14 s^{-1}	0.25	10	14.3	1.4
Shear flow, 0.83 s^{-1}	1.5	10	14.3	1.4

situations occurring in industrial or biomedical fields, because biofilm formation occurs in stagnant conditions. Moreover, the lack of a continuous feed of fresh medium can lead to nutrient limitations.

Experimental set-ups for biofilm cultivation in dynamic conditions have also been assessed. Despite the simplicity of these systems, the established hydrodynamic conditions are not easily predictable. Therefore, chemostatic and continuous flow devices have recently gained more attention. Rotating disk reactors are used for biofilm cultivation for their high throughputs, and for the possibility to operate at a wide range of shear conditions. Drip flow reactors accommodate very slow flows driven by gravity; however, their geometrical features do not allow to replicate actual pipe/channel flows and to monitor biofilm growth *in-situ*/on-line. In addition, their cost remains relatively high [18]. Flow chamber reactors have been widely used to investigate biofilm formation and morphologies under well controlled hydrodynamic conditions [19–23], because of their capability to monitor non-invasively the growth, structure, and physiology of such biological systems over time. Moreover, compared to the previous growth techniques, flow-through configurations provide easily steady state conditions. Nowadays, different flow camber designs are employed to study biofilm growth and detachment under the action of flow either on macroscopic or microscopic (microfluidics) scales. Although a lot of research has been conducted to study biofilms under different *in vitro* conditions, a meticulous comparison among different culture conditions is still lacking in literature.

In this work, *Pseudomonas fluorescens* AR 11 cultivated on glass coupons is used as a model system of single-strain biofilm. *P. fluorescens* is a Gram-negative, rod-shaped aerobic bacterium, well-known to form biofilms [24].

We compare quantitatively three different *in vitro* growth techniques corresponding to three different flow conditions: (i) stagnant conditions (unstirred batches, no flow), (ii) shaken vessels (full agitation), and (iii) a custom-made rectangular flow chamber (controlled laminar flow). The effect of flow on biofilm morphology is investigated. Each method is characterized by the exposure of the growing biofilm to different values of shear rate but also to different profiles in time and space of concentrations of nutrients and metabolites. In stagnant conditions, a concentration profile of nutrients is expected to gradually develop towards the biofilm surface until the nutrients get fully depleted at some point during the tests. In shaken conditions, the agitation yields a uniform concentration of nutrients in the culture chamber and in addition nutrients are replenished after certain hours to avoid depletion. Finally, in the flow chamber the low retention time warrants that nutrients are always available and so both planktonic and adhering cells are in active physiological state (*i.e.* growing) during the observation time.

Apart from conventional growth and morphological properties, wetting is investigated too, to assess the interaction between biological coatings and either hydrophilic or lipophilic fluids with the final goal to find strategies to remove or prevent the formation of detrimental biofilms.

Recent literature has been reported that biofilms, grown at solid-air interfaces (Agar substrates), are capable to resist to a wide of antimicrobial and cleaning agents [25–27] showing both hydrophilic and hydrophobic wetting behaviours, according to the biofilm-forming strains and the selected nutrient conditions [27]. Interesting results claim that the biofilm wetting properties depend on the biofilm topography. In this field, exploratory wetting experiments are performed on biofilm formed on real solid surfaces (i.e glass coupons).

2. Materials and methods

2.1. Bacterial strain and culture media

Lyophilised bacterial cells, purchased from DMSZ (Braunschweig, Germany), are rehydrated and grown at 30 °C in a liquid complex medium, made of 5 g of peptone from animal tissue and 3 g of meat extract per litre of bi-distilled water according to the protocol suggested by the supplier [28]. Bacterial suspensions are standardised by dilution to reach an optical density (OD_{600nm}) ≈ 0.5, which corresponds to $4{\cdot}10^7$ microorganisms/mL, approximately.

For biofilm cultivation, M9 minimal medium is selected (consisting of 6.8 g/L of $NaHPO_4$, 3 g/L of KH_2PO_4, 0.5 g/L of NaCl and 1 g/L NH_4Cl, 95 mg/mL $MgSO_4{\cdot}7H_2O$, 5.85 mg/mL $CaCl_2{\cdot}2H_2O$, 0.198 g/mL EDTA, 2 mg/mL $FeCl_3$ .6 H_2O, 0.21 mg/mL $ZnCl_2$, 0.03 mg/mL $CuCl_2{\cdot}2H_2O$, 0.025 mg/mL $CoCl_2{\cdot}2H_2O$, 0.025 mg/mL H_3BO_3 and 0.004 mg/mL $MnCl_2{\cdot}4$ H_2O and 0.4 % succinic acid) at pH 7.

2.2. Biofilm growth experiments

For biofilm cultivation, three different *in vitro* techniques are employed: two batch techniques (stagnant fluid and shaken vessels) and a custom-made continuous flow technique. Experiments are carried out within an overall incubation time of 72 h, which is the time corresponding to the biofilm maturation phase. Process and geometrical parameters of each *in vitro* technique are summarised in Table 1. The three experimental set-ups are shown in Fig. 1.

2.2.1. Stagnant fluid

Biofilms are cultivated over optical glass coupons (1.8 × 1.8 cm) at 30 °C, placed inside 12 aerated well-microplates. Temperature of experiments is selected so as to provide optimum conditions for the specific bacterial strain growth, according to the protocol suggested by the supplier [28]. A glass coupon, 1.8 mL of sterile minimal medium and 200 µL of inoculum (1:10 dilution) are inserted in each well. Biofilm is formed on both sides of the glass coupons, the total surface area of each glass coupon is 6.48 cm^2 and the ratio of active surface/total volume of each well is 8.5 cm^{-1}. Active surface area includes also side walls (Table 1).

2.2.2. Shaken vessels

Biofilms are cultivated over optical glass slides (7.6cm × 2.6cm) placed in tilted 50 mL Falcon tubes. Each Falcon tube is filled with 18 mL of sterile minimal medium and inoculum (1:10 dilution) and then it is placed on an oscillating plate (90 rpm) of a shaking incubator at 30 °C. Temperature of experiments is selected so as to provide optimum conditions for the specific bacterial strain growth, according to the protocol suggested by the supplier [28]. After 24 h of incubation the turbidity of the medium increases considerably (to about 1.0 cm^{-1}), implying rapid lack of food and approach of death phase of the bacteria, so it is decided to replace the nutrients every 24 h. For shaken vessels, the surface area of glass coupon is 39. 5 cm^2 (considering both sides of

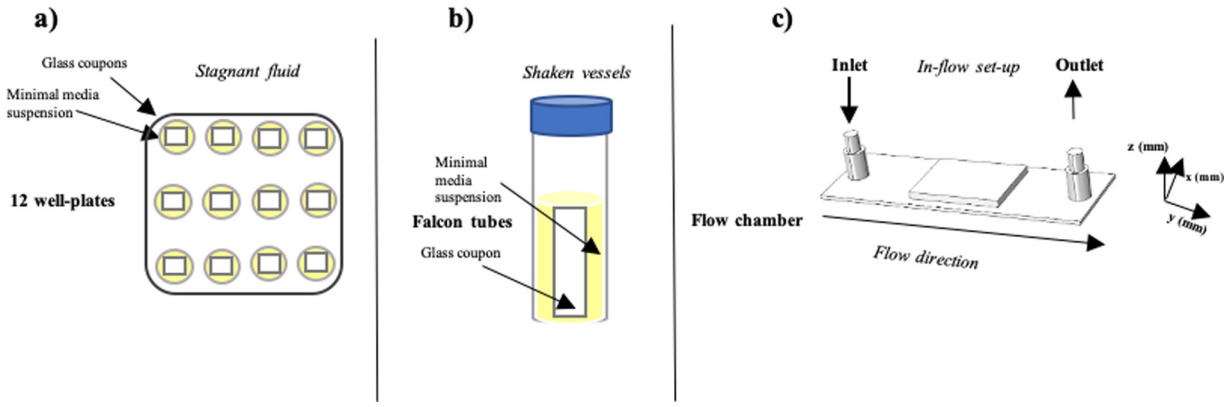

Fig. 1. Experimental set-ups for: a) batch tests with stagnant fluid conditions, b) batch tests with shaken vessels and c) continuous, in-flow experiment.

glass coupon, Table 1). However, the actual ratio of active surface area and total liquid volume is only 6.7 cm^{-1} which is comparable to the value for stagnant fluid (8.5 cm^{-1}). In this case, the shear rate at the wall as function of time, $\dot{\gamma}_w(0, t)$, for unsteady laminar flow near an oscillating plate also show sinusoidal trend. A rough estimation suggests the shear rate imposed at the wall variates over time in the range 0-10 s^{-1}.

2.2.3. Flow chamber apparatus

A flow apparatus (Figure S1, supplementary materials), is homemade with the aim to study biofilm formation under controlled hydrodynamic conditions.

The flow chamber is made of two stainless steel plates, hosting a microscope slide onto which biofilms are formed. The internal free volume of the channel occupied by the flowing liquid is 30 mm^3. Details of the experimental procedures, and flow chamber, are reported in the supplementary (S1), together with a numerical analysis of the flow conditions (S2).

For a laminar flow in a narrow slit (of half-thickness δ along the z direction), with the slit width (W, along the x direction) W > > δ, the velocity field (along the y direction) can be estimated by the following equation [29]:

$$v_y = \frac{3}{2} \bullet v \bullet \left(1 - \left(\frac{z}{\delta}\right)^2\right) \quad (1)$$

where v is the average volumetric velocity in the flow channel.

In this work, two different volumetric flow rates (Q = 0.25 mL/min and 1.5 mL/min, corresponding to $\dot{\gamma}_w$ = 0.14 s^{-1} and 0.83 s^{-1}) are tested to investigate biofilm formation under two different flow conditions, both in the laminar regime. According to Eq. (1), the shear rate at the wall ($z = \pm \delta$), can be estimated from Eq. (2):

$$\dot{\gamma}_w = \left| \frac{dv_y}{dz}\bigg|_{z=\pm\delta} \right| = \frac{3Q}{(2\delta^2 \bullet W)} \quad (2)$$

Reynolds numbers, Re, evaluated according to Eq. (3), are equal to 1.4 and 8.3, respectively, for the two flow conditions.

$$\mathrm{Re}_{D_h} = \frac{\rho \bullet v \bullet D_h}{\eta} \quad (3)$$

where ρ is the density (kg • m^{-3}), η is the kinematic viscosity (Pa • s) of the growth medium and D_h is the hydraulic diameter, evaluated as 4 times the ratio of the cross-sectional area over the wetted perimeter.

$$D_h = \frac{4A}{P} = \frac{4(W \cdot \delta)}{W + 2\delta} \quad (4)$$

For the flow chamber of this work, W = 20 mm and δ = 1.5 mm.

2.3. Planktonic and biofilm growth

Planktonic and biofilm kinetics of growth are assessed by spectrophometric methods.

Number of bacterial per unit of volume (counts/mL) can be estimated by measuring the optical absorbance at 600 nm [30]. A calibration curve of OD600 *vs* cell density is provided in Figure S3 (supplementary materials). 1 mL of suspension is withdrawn at defined time intervals and gently homogenised by vortexing before measuring OD_{600}.

In the specific case of the flow chamber, bacterial suspension is collected at the chamber outlet.

The crystal violet assay is used to assess the biomass attachment, according to the protocol suggested by [31]. Glass coupons are stained with 0.1 % crystal violet solution and incubated for 10 min and then rinsed twice with bi-distilled water to remove excess stain solution. Next, crystal violet from stained cells is solubilized with 50 % (v/v) ethanol/water solution for 10 min. The optical density of resulting crystal violet solution is measured at 570 nm to quantify the biomass attached onto glass substrates at regular time intervals.

Experiments are performed in triplicate.

2.4. Biofilm imaging and analysis

Biofilm morphology is assessed *via* Confocal Scanning Laser Microscopy (CSLM), performing a Double staining. Bacterial cells are stained using the green fluorescent dye, SYTO® 9 (from LIVE/DEAD™ Biofilm Viability Kit, Molecular Probes, Invitrogen, Carlsbad, CA, USA). A staining solution is prepared by adding 3 µL of SYTO® 9 stain in 1 mL of sterile bi-distilled water. On the other hand, the red fluorescent dye, TRITC conjugate CoA (Tetra-methyl-rhodamine conjugated Concanavalin A, Molecular Probes, Invitrogen, Carlsbad, CA, USA) at 100 µg/mL in sterile bi-distilled water, is used to stain α-mannose residues within biofilm matrix. Samples are incubated with 200 µL of staining solutions in the darkness for 30 min at room temperature. Rinsing with bi-distilled water is carried out to remove excess stain.

Images are acquired by using an inverted microscope (Nikon Eclipse Ti E, Nikon Corporation, Japan), Images are taken using a Plan Apo λ 40 X/1.49 NA air-objective and a Nikon digital camera. Excitation of samples is provided by an Ar laser at the wavelength of 488.6 nm using a detection filter of 498 nm and a He-Ne one at the wavelength of 561.5 nm with a detection filter of 580 nm. Image z-stacks are acquired using 0.5 µm intervals at three different positions within each sample (26 cm, 40 cm and 50 cm from the inlet), recorded as series of TIFF files, and processed by NIS-Elements Imaging Software. Image stacks having a XY area of about 10^5 μm^2 (316.76 × 316.76 µm) are selected. Samples are imaged along the z-direction for their entire sample thickness. For processing stacks images, the auto-thresholding procedure based on the well-known Otsu's method [32] is selected, by providing threshold

values in the range of 65 − 85.

Image processing is performed by COMSTAT 2, a MATLAB© script, developed by Heydorn et al. [33], which is developed to run in the free-software Image J by Vorregaard [34].

Both green and red channel image stacks are processed. Cell biomass ($\mu m^3/\mu m^2$), defined as the sum of number of voxels occupied by cells in each horizontal plane, is acquired from green-channel-image stacks. Analysis of red-channel-image stacks provides a measure of surface area (μm^2) (area occupied by biofilms), biofilm thickness (μm), and roughness coefficient, Ra (nondimensional index measuring biofilm heterogeneity). Ra is evaluated according to the Eq. (5), where L_i is the i-th individual thickness measurement (μm), L_F is the mean thickness (μm) and N is the number of thickness measurements.

$$R_a = \frac{1}{N}\sum_{i=1}^{N}\left|\frac{L_i - L_F}{L_F}\right| \quad (5)$$

2.5. Wetting analysis

Wettability experiments are conducted to investigate the hydrophilic and lipophilic nature of biofilms surface, using bi-distilled water and soybean oil (S7381 from Sigma Aldrich), as wetting agents. Biofilm coated glass coupons are pre-conditioned for 24 h, in a sealed cylindrical chamber (90 mm diameter, 150 mm length) to avoid air flow and contamination by fresh air. Tests are performed at room temperature 25 ± 2 °C. Tests conducted under controlled relative humidity conditions of 75 % and 100 %, obtained by using saturated salt solutions of NaCl and water, respectively, and are also investigated to assess the effect of the relative humidity on biofilm wetting properties.

After preconditioning, 20 μL-droplets are gently deposited onto biofilm surfaces by microliter syringe (Hamilton, Reno, NV, USA). Top and side views of droplets are obtained using a digital camera on a tripod (Canon EOS 60D, Canon) equipped with Canon EF-S 60 mm Macro Lens. Sessile drop contact angle measurements are performed by image analysis. It should be pointed out that the choice of the volume droplet does not affect the contact angle values, since the contact angle is a physical property of liquid-solid systems. The droplet volume plays a role only in droplet sphericity, which reflects on the surface tension. However, this aspect is not examined, as it tallies beyond the scope of this work.

Experiments are carried out at least in triplicate, *i.e.* for each growth condition at least 3 independent samples are used, whereas on each sample independent measurements are done placing different droplets at different positions across the sample surface. The data reported are the average of all the measurements, error bars are calculated as the standard error of the mean. Image processing to obtain angle values is performed using a commercial package software (Image Pro Plus 6.0, Media Cybernetics, Rockville, MD, USA).

3. Results

3.1. Biofilm growth kinetics under different flow conditions

3.1.1. Biofilm growth kinetics in batch modes (stagnant and shaken)

Biofilms are cultivated under different growth conditions, as described in the experimental section. In Fig. 2(a), kinetic growth curves are reported as a function of the growth time in either stagnant or shaken fluid. The analysis of *P. fluorescens* biofilm formation over time presents the typical curve of biofilm formation. Typically, it is possible to distinguish four phases of biofilm formation (initial lag phase, log growth phase, steady state phase and death phase).

In stagnant fluid conditions, the selected bacterial strain shows a lag-phase of less than 1 h and a log-phase of about 2 days. (Fig. 2(a), red squares). Planktonic biomass growth in the suspended medium starts just after the inoculation period and reaches a plateau after 24 h. This suggests that around this time C-source and/or nutrients get depleted. At 72 h there is a slight decrease in $OD_{600\ nm,}$ probably due to the beginning of the death phase. Biomass attached on glass surfaces (*i.e.*, the formed biofilm), shows a similar trend as cell adhesion is already observed after 3 h from the inoculation (Fig. 2(b), red squares). Typically, the qualitative trend of biofilm biomass growth *versus* time is similar to planktonic biomass.

In shaken vessels, the turbidity of the medium shows a faster increase respect to the stagnant conditions and, due to nutrients depletion, medium has to be replaced every 24 h (Fig. 2(a), blue circles). Due to nutrients replacement and thus the restoration of the initial conditions, indications of cell death phase are not present. The faster biomass growth is attributed to the agitation of medium during shaking, which facilitates the transport of oxygen and nutrients. The planktonic growth from 48 to 52 h, expressed in terms of OD_{600nm}, is surprisingly higher when compared to the growth of planktonic bacteria from 24 to 28 h or to that from 0 to 4 h. Yet, the overall planktonic population growth after 24 h of each replacement presents just a slight increase, which is not expected to affect the overall development of the biofilm, since the OD_{600nm} is close to 1 cm^{-1}. Moreover, the nutrient replacement produces an oscillation in the $OD_{570nm,}$ which is proportional to biofilm biomass, with a periodicity of 24 h (Fig. 2(b), blue circles). The oscillation is basically due to medium replacement. It might have been expected that nutrients and carbon source replacement enhance the biofilm development, however the decrease of OD_{570nm} indicates that the replacement causes partial detachment of some attached bacteria. This behaviour is observed most probably due to poor adhesion of these cells to the biofilm structure. Nevertheless, the final biofilm biomass is slightly higher in shaken medium with periodic replacement. In addition, the partial detachment of bacteria from biofilms may induce the increase of the optical density of planktonic cells at 28, 52 and 72 h as it is displayed in Fig. 2b (blue plot).

3.1.2. Biofilm growth kinetics in the flow chamber

In Fig. 2(c), the turbidity of the effluent is reported as a function of time for two different hydrodynamic conditions. It is worth mentioning that in the flow chamber used in this work, nutrients are always abundant because of the low retention time. The observed turbidity of the effluent is due to detachment of biomass from biofilm and possible subsequent planktonic growth during the examined retention times.

Attached biofilm biomass on samples growth in the flow chamber apparatus is evaluated only at the end of the experiments (inset plot in Fig. 2c). After 72 h of operation, glass coupons are withdrawn and stained with crystal violet, according to the procedures described in the experimental section. 3-fold-reduction of optical density at 570 nm is achieved with increasing shear rate from 0.14 to 0.83 s^{-1}. At the same incubation time (72 h), biofilms cultivated under low shear rate conditions ($\dot{\gamma}_w = 0.14\ s^{-1}$) show a higher accumulation of biomass onto glass surfaces (evaluated as OD_{570nm}) than biofilms developed in stagnant or in shaken conditions. However, at increased shear rate ($\dot{\gamma}_w = 0.83\ s^{-1}$), OD_{570nm} is instead comparable to the ones obtained in batch conditions. These results will be further analyzed in the following discussion section.

3.2. Biofilm morphology under different flow conditions

Pseudomonas fluorescens biofilms show different 3D structures, depending on the growth conditions. In Fig. 3, CSLM merged stack images are reported as measured for the different set-ups.

After 72 h, under stagnant conditions (Fig. 3a), biofilms present of isolated cells and colonies.

In shaken fluid conditions (Fig. 3b), biofilms show clearly bacterial clumps (green colour), whose formation is due to the imposed agitation. Compared to biofilms cultivated in stagnant fluid, biofilms under shaking conditions appear thinner, probably because of shear induced erosion. It is known [35,36] that strong flows can induce erosion and

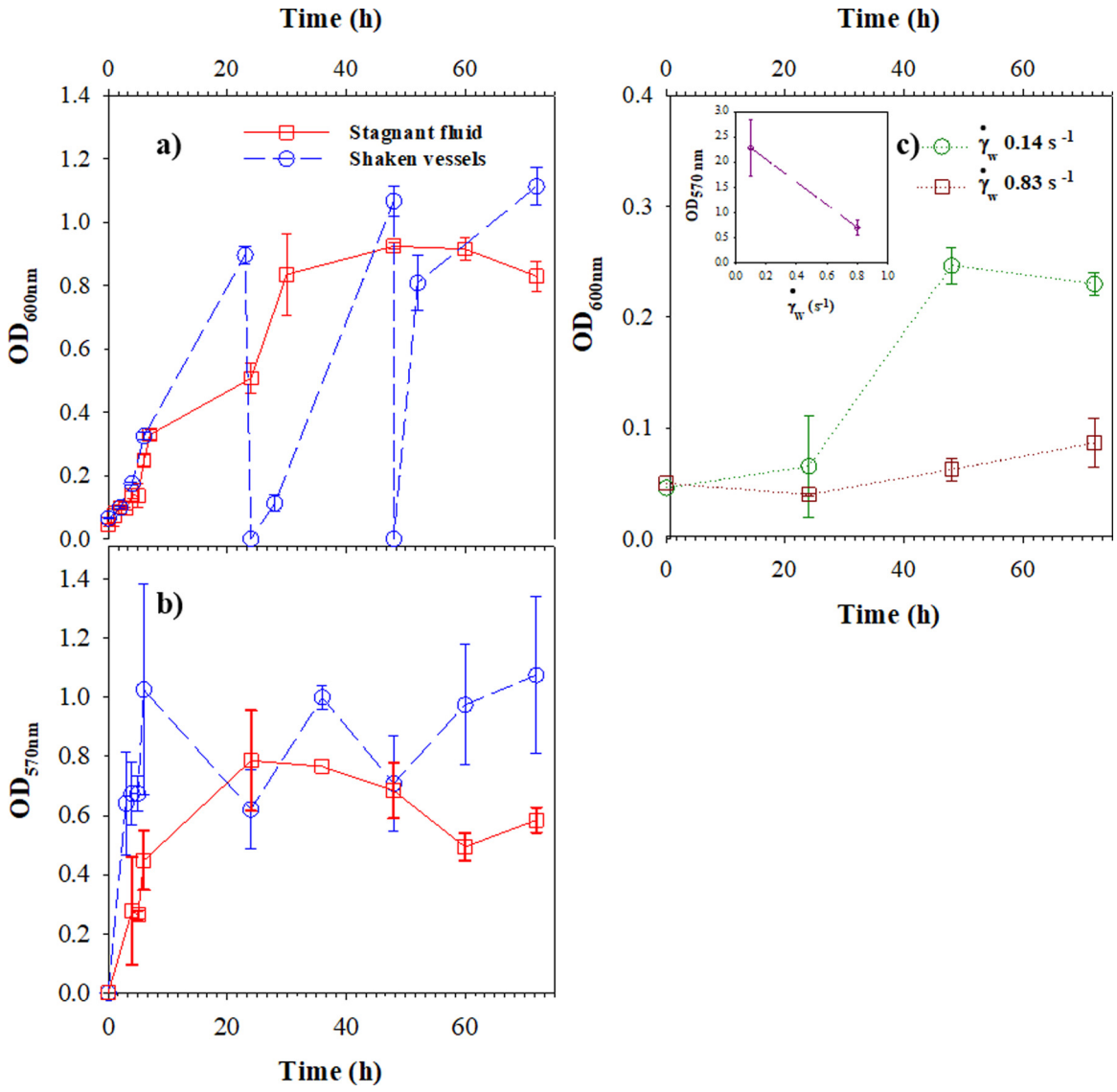

Fig. 2. Turbidity measurements are used as a measurement of bacterial growth under different flow conditions. (a) Turbidity of suspended planktonic biomass as function of incubation time for stagnant and shaken fluid conditions. (b) Turbidity of the attached biofilm biomass evaluated *via* crystal violet assay, as function of incubation time for stagnant and shaken fluid conditions. (c) Turbidity, due to biomass detachment and growth, measured at the outlet of the flow cell as a function of time under the two shear rates of $\dot{\gamma}_w$ = 0.14 and 0.83 s^{-1}. (c) Inset: Attached biofilm biomass, evaluated *via* crystal violet assay, after 72 h, for the same shear rates. Standard deviations from triplicate independent experimental reproducibility are reported as error bars.

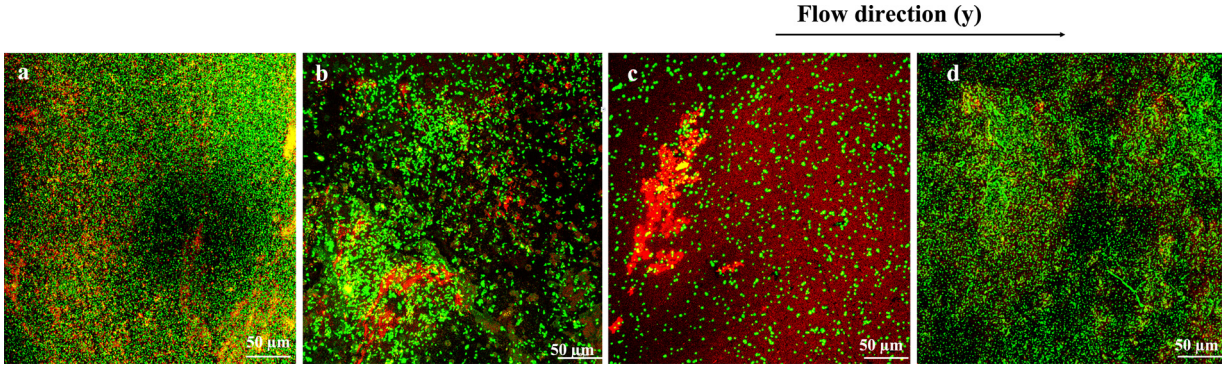

Fig. 3. Orthogonal projections of CSLM stack images of 72 h biofilms, cultivated in different *in vitro* set-ups. a) stagnant fluid, b) shaken vessel, c-d) well-controlled flow conditions ($\dot{\gamma}_w$ = 0.14 and 0.83 s^{-1} respectively). Samples are double stained: Bacteria cells are stained with green fluorescent dye, SYTO® 9 and biofilm α-mannose residues are stained with TRITC conjugated Concanavalin A, in red channel. 40 X magnification. Scale bar: 50 µm.

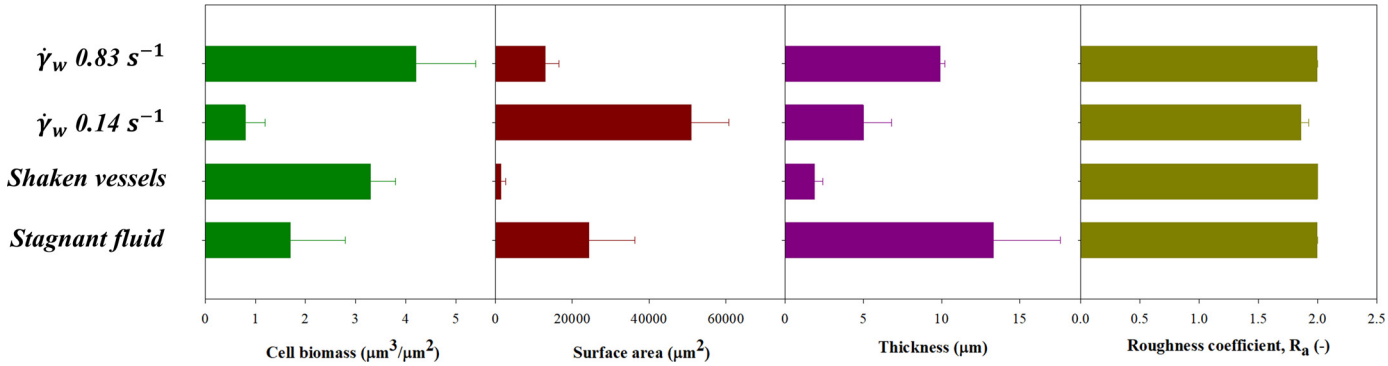

Fig. 4. Morphological parameters evaluated by processing CSLM stack images of biofilms, cultivated under different flow conditions: stagnant fluid, shaken vessels and well-controlled hydrodynamic conditions ($\dot{\gamma}_w$ = 0.14 and 0.83 s^{-1}). Average values ± standard deviation, calculated from of at least triplicate independent experiments are shown.

detachment, due to the effect of shear stress. The quasi-periodical change of shear conditions induces patchy structures, made of bunches of bacterial clumps randomly attached on the substratum and separated by empty spaces. Moreover, shaken fluid conditions seem to be detrimental to the formation of the exo-polymer matrix, as suggested by the fact that red fluorescent signal is lower than the green one in the images analysed here.

Concerning the experiments using the flow chamber (Fig. 3c and d), CSLM images show different spatial patterns according to the different imposed hydrodynamic conditions. At the lower shear rate ($\dot{\gamma}_w$ = 0.14 s^{-1}, Fig. 3c), clumps uniformly distributed along the surface are predominant. Under higher shear rate ($\dot{\gamma}_w$ = 0.83 s^{-1}, Fig. 3d) biofilm shows filamentous and elongated, tower-like structures, where bacterial cells are mainly distributed on the upper layer, while compact EPS are located closed to the substratum.

Confocal stack-images are analysed to quantify parameters specific parameters of biofilm morphology: cell biomass, biofilm thickness, surface area occupied by biofilms and roughness coefficient. In Fig. 4, horizontal bars report the value of different morphological parameters, averaged over at least 3 independent measurements, the standard deviation is reported as error bar.

Stagnant fluid biofilms are not particularly cell dense, but strongly developed in height, with biofilm surface area corresponding to surface coverage of 24.3 %. Under shaken flow, cell biomass is two times higher compared to stagnant conditions, but with severely reduced thickness. Surface area covered by biofilms is also reduced from 24.3 % to 14 %. Overall, shaking seems to induce flattening of biofilm structures and to promote bacterial aggregation.

Under well-controlled flow conditions, biofilms morphology show specific trends as function of the shear rate, in the range here considered. Cell biomass increases with the imposed shear rate. Biofilm thickness increases by almost 50 %. On the contrary, surface area covered by biofilm drops as shear rate increases, reducing of a factor 74.5 %. Roughness coefficient slightly increases when increasing the shear rate, due to shear flow. However, among all the examined morphological parameters, the roughness coefficient exhibits the smallest variation among flow conditions implying that in the examined range of values the shear does not affect significantly this aspect of the morphology of the exposed biofilm surface, despite the shear induced erosion can induce severe reduction in sample thickness.

3.3. Wetting analysis

Exploratory wetting analysis of biofilms cultivated under different flow conditions is summarized in Fig. 5, where top and side views of 20 μL droplets deposited onto biofilms, cultivated under different flow conditions using a RH 100 % are reported. A comparison with untreated glass samples (without attached biofilms) is also reported for comparison.

Pseudomonas fluorescens biofilms grown on glass coupons are more hydrophilic than the untreated control, showing contact angle values in the range 20°–30° (Fig. 5b, blue-bars), with the bare glass coupons showing an average static contact angle about 68°, which is higher than other measurements reported in literature. It is worth mentioning there is quite a broad range of values measured in the literature (40°-60°) [37,38]. This apparent disagreement is probably due to different cleaning procedures. What is of great interest is the peculiar behaviour of water droplets onto biofilms manifested by the observed irregular and jagged contours, while water droplets onto uncoated glass coupons show the expected spherical shape. This might be due to the physical-chemical interactions (*i.e.* OH-bonds) between water and EPS of polymeric matrix and is expected to heavily affect the performance of cleaning solutions in removing the biofilms from solid surfaces.

Biofilms also show a good compatibility with a biological oil such as soybean oil. This is evident by measures of static contact angles onto biofilms in the range 30°-40° (Fig. 5, red-bars) showing the same trend respect with bare glasses (which is about 50°). This might be related to either the presence of phosphate groups of phospholipidic chain in soybean oil or to some other molecular interaction between the biomass and soybean-oil.

In both cases (hydrophilic and lipophilic liquids), one can argue that the different flow conditions experienced during biofilm formation does not influence significantly the wetting properties of biofilms. Specifically, for the water/biofilm system it can be further argued that as shear rate increases, the static contact angle decreases. Considering morphology measurements reported in Fig. 5, this might be ascribed to the presence of a greater amount of biofilms (cell biomass and thickness) on the solid substrate. The present results are in line with contact angles of microbial lawns experimentally reported by van der Mei et al. [39] for which contact angles of *Pseudomonas fluorescens* with polar fluids (i.e water) are comparable with those with apolar fluids (i.e α-Bromonaphthalene).

The influence of relative humidity on wetting properties of biofilms is also investigated, for the case of biofilm cultivated in batch modes. In Fig. 6, the static contact angles on biofilms with two different relative humidity (100 % and 75 %) are reported. As reported in Fig. 6b, and the static contact angles of both water and soybean oil is affected by the different relative humidity. Biofilm cultivated under stagnant fluid conditions show a slight increase in water contact angle with relative humidity. The opposite trend is found for water contact angles on biofilm cultivated in shaken vessels. Soybean oil contact angles decrease with relative humidity for both stagnant fluid and shaken vessels. This might be due to the adsorption of some water molecules on the glass surfaces.

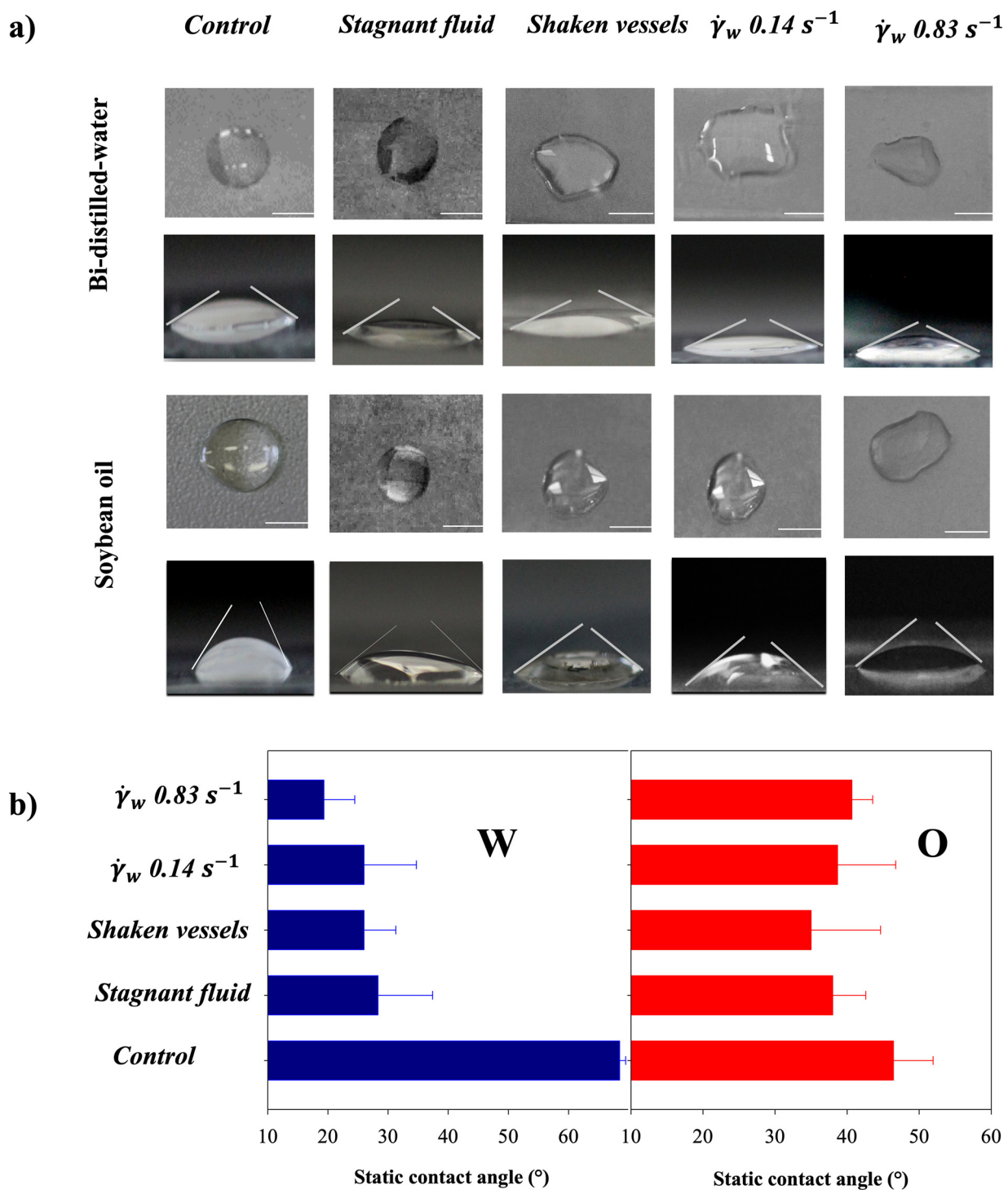

Fig. 5. a) Top and side views of 20 μL droplet of water (above) and soybean oil (below). Scale bar: 4 mm b) Static contact angles of water (blue-bars left-plot, denoted as W) and soybean oil (red-bars right-plot, denoted as O) on biofilm coated glass coupons under different flow conditions.

4. Discussion

In this work, *Pseudomonas fluorescens* biofilms are cultivated under three different flow conditions *i.e.* stagnant fluid, shaken fluid and well controlled laminar flow conditions inside a custom-made flow chamber. The role of flow on biofilm growth is evaluated with respect to biomass growth curves as well as in terms of biofilms morphological and wetting properties.

A custom orthogonal cross-section slit flow apparatus has been used to study the biofilm growth and the morphological patterns induced by flow. Using this configuration, it has been possible to impose controlled velocity fields and control shear rate on sample surface. Two distinct hydrodynamic conditions are evaluated, corresponding to wall shear rates equal to 0.14 s^{-1} and 0.83 s^{-1}, respectively. Reynolds numbers, evaluated according to Eq. (3), are equal to 1.4 and 8.3, which corresponds to flow conditions typical of flow systems such as small pipes and industrial filters or medical devices [40].

Under stagnant conditions, where diffusion is likely to be the controlling resistance in nutrient transport, biomass probably grows in the first hours from inoculation and then tends to agglomerate at longer

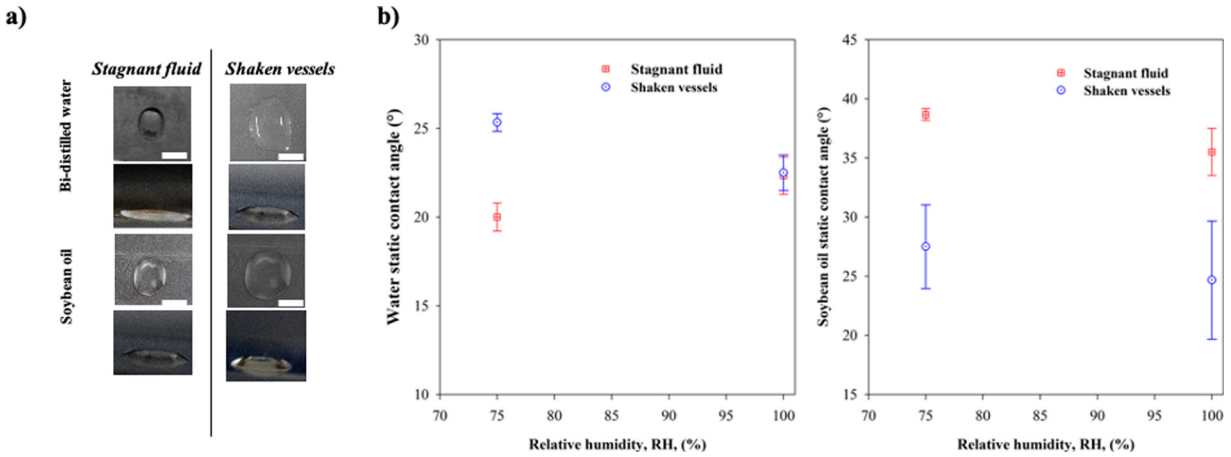

Fig. 6. a) Top and side views of 20 µL droplet of water (above) and soybean oil (below) at RH 75 %. Scale bar: 4 mm b) Static contact angles of water and soybean oil onto biofilm coated glass coupons cultivated under batch conditions as function of relative humidity.

times, when nutrients are depleted. Under shaken conditions, where nutrient medium is periodically replaced, the main transport mechanism is the fluid convection due to agitation. Flow is not easy to analyse and is strongly variable over time. Under these conditions, biofilm growth can be expected to be the result of a balance between sloughing off and regrowth phenomena, induced by the agitation flow.

It has not been possible to evaluate quantitatively biofilm growth rate *versus* time, but a qualitative estimate has been made by measuring the crystal violet OD_{570nm} with time, which is an indirect measure of biofilm mass growth. More specifically, under stagnant flow conditions, crystal violet OD_{570nm} reaches a maximum at around 24 h, being followed by a plateau phase for the next 12 h. In shaken flow, the frequent replacement of the nutrient medium induces an oscillation in the crystal violet OD_{570nm} signal, but the final value reached after 72 h is higher respect the case of stagnant conditions.

Concerning biofilm growth under well controlled laminar flow conditions in the custom flow chamber, biofilm biomass is evaluated only at the end of each run (72 h). It is found that OD_{570nm} at 72 h decreases as shear rate increases.

In continuous flow, at steady state conditions, it is possible to interpret the phenomenology of biofilm growth according to a transport-phenomena approach.

Mass transfer Biot number Bi_m, is evaluated by Eq. (6) to compare bulk convection rate with diffusion rate within the biofilm.

$$Bi_m = \frac{k_c \bullet \delta_B}{D} \tag{6}$$

where k_c is the convective mass transfer coefficient (m/s), and D is the effective diffusion coefficient (m^2/s) and δ_B is the biofilm thickness (µm), evaluated by image analysis for the two flow conditions. As order of magnitude estimate, it can be assumed that the diffusion coefficients of small solutes such as oxygen and succinic acid in water are of order of 10^{-9} m^2/s at ambient temperature [41] and the biofilm thickness δ_B is about 10 µm. The coefficient k_c is evaluated locally with respect to the center of the glass window, by assuming laminar flow through a rectangular duct by Eq. (7) [42]:

$$\frac{k_c \bullet y_m}{D} = 1.62 \bullet \left(\frac{D_h^2 \cdot v}{y_m \cdot D}\right)^{1/3} \tag{7}$$

where S_h is the Sherwood number, y_m is the medium length (m), D is the diffusion coefficient (m^2/s), D_h is the hydraulic diameter (m), v is the average velocity in the rectangular duct (m/s). The results of the calculations are summarized in Table 2.

The estimated values of Bi_m are $4.6 \bullet 10^{-3}$ and $8.4 \bullet 10^{-3}$, for $\dot{\gamma}_w = 0.14\ s^{-1}$ and $\dot{\gamma}_w = 0.83\ s^{-1}$, respectively. Therefore, in both cases, the external mass transfer resistance can be considered the controlling slow step. This agrees with previous results from Stewart [41], which found that specific morphological patterns induced by the flow are recognized when the external mass resistance is not negligible. More specifically, under slow flow, column like structures are present in the biofilm, which develop following to a nutrient concentration gradient [41]. Thomen et al. [43] found no direct impact of mechanical forces on biofilm growth rate. On the other hand, they demonstrated that hydrodynamic conditions influence the molecular transport and the oxygen availability. Therefore, at increased shear rate conditions, biofilm formation is enhanced due to the higher delivery of oxygen and nutrients to bacterial cells constituting biofilms. The above observation is in line with the results presented in Fig. 3 about the dependence of biofilm thickness and surface area on shear rate.

As pointed out in the Results section, different flow conditions induce different morphologies in bacterial biofilms. Under stagnant conditions, biofilms are porous structures, mostly developed in height. This peculiar morphology could be associated to the stagnant conditions in which the diffusion is the only relevant mass transfer mechanism, causing nutrient depletion and enrichment of waste products within biofilms. Under shaken flow conditions, no specific morphological pattern is recognized, and biofilms are thinner than the ones obtained in stagnant medium conditions.

Under laminar flow conditions, specific morphological patterns are recognized. At lower shear rate, clumped or single cluster-like structures are predominant, and it has not been possible to observe a conspicuous formation of biofilm matrix EPS, especially in terms of thickness.

By increasing shear rates, biofilms are filamentous and elongated,

Table 2
Experimental conditions during tests at different flow conditions.

Flow rate (mL/min)	Retention time (min)	$\dot{\gamma}_w$ (s^{-1})	Re (-)	τ_w (Pa)	Sh (-)	k_c (m/s)	Bi_m (-)
0.25	12	0.14	1.39	$1.39 \cdot 10^{-4}$	15	$4.6 \cdot 10^{-7}$	$2.3 \cdot 10^{-3}$
1.5	2	0.83	8.33	$8.33 \cdot 10^{-4}$	28	$8.33 \cdot 10^{-7}$	$8.4 \cdot 10^{-3}$

with denser, thicker and more wrinkled structures. Similar results are shown in previous studies [44,45]. These results seem to be in contrast with the findings from the crystal violet assay, which show a lower value of OD_{570nm}, and thus of the amount of attached biomass, at higher shear rate. A possible explanation of such discrepancy is that crystal violet is not a viable marker, since it is able to stain both bacterial cells and EPS [46] and even dead cells and debris. This is particularly evident at lower shear rates, where the flow fails to yield an efficient mass transfer within biofilms and the presence of dead cells might be noticeable. For these reasons, quantification of CSLM stacks remains more reliable than spectrophotometric assays for biofilm characterization. Moreover, biofilms cultivated under laminar flow seem to be less developed in height than biofilms cultivated in stagnant conditions.

The influence of the detachment induced by the flow under the applied hydrodynamic conditions used is also evaluated. The wall shear stress, τ_w,(Pa) can be estimated from Eq. (8).

$$\tau_w = \dot{\gamma}_w \bullet \eta = \frac{3Q}{(2\delta^2 \bullet W)} \bullet \eta \quad (8)$$

Where η is viscosity of the growth medium, which can be approximated by that of water ($\eta = 10^{-3}$ Pa • s). For the selected hydrodynamic conditions, it is found that τ_w is $1.4 \bullet 10^{-4}$ Pa and $8.3 \bullet 10^{-4}$ Pa, for $\dot{\gamma}_w$ 0.14 s^{-1} and 0.83 s^{-1}, respectively. It has been shown that *Pseudomonas aeruginosa* completely detaches under a wall shear stress value around 10^{-2} Pa [22]. Therefore, the selected hydrodynamic conditions are below the critical value for the wall stress to detach the biofilm. In fact, the selected operating conditions are two and one order of magnitude less than the ones used in previous studies ([47–49]. This difference makes it difficult to compare our results with those reported in the literature, such as that *P. fluorescens* biofilms under laminar flow show more viable biomass at increased flow rate [48,50] and that biofilms under higher flow velocity are thinner, with a reduced content of EPS due to mechanical shear [50]. Therefore, an extension of this study is needed to explore a wider range of shear conditions.

The wettability properties of biofilm-coated coupons are investigated, too, using two different wetting agents: bi-distilled water and soybean oil. To carry out wetting experiments, process parameters such as volume of the droplets, air relative humidity, and temperature, are kept constant.

The phenomena of biofilm wetting are still poorly understood. More specifically, a lot of work has been devoted to assess the bacterial adhesion to surfaces [39,51] and the initial bacterial transport phenomena such as bacterial mass transport to surface, reversible adhesion and the transition between reversible and irreversible adhesion [52]. Wetting properties of *Bacillus subtilis* Agar colonies have been investigated by Epstein et al., Werb et al. and Falcón García et al. [25–27] who demonstrated that wetting properties are synergistic results of biofilm composition, microstructures, roughness [25] and growth media type and composition [26,26,27].

This work has demonstrated that biofilm-coated glass-substrates are more hydrophilic than bare (uncoated) controls, with a good capability to interact with biological oils, such as soybean oil. A possible explanation of this amphiphilic behavior might be related to the biofilm matrix composition. Biofilm matrix is actually a porous network, made of EPS, able to adsorb water, inorganic ions and organic compounds. Therefore, biofilms show adaptable wetting properties, since they can interact also with hydrophobic fluids. For this reason, biofilms are able to adapt themselves to different hostile environments (such as humid places). Although it is shown herein that biofilm wetting properties do not depend significantly on flow conditions, further work is needed to elucidate the interfacial properties of bacterial biofilms.

5. Conclusions

In this work, a comparison among three *in vitro* set-ups for biofilm cultivation is performed, corresponding to three flow conditions *i.e.* stagnant fluid, shaken fluid and well-defined laminar flow conditions. In this latter case a custom-made flow chamber is used to assess biofilm formation under controlled velocity gradients. The role of flow on growth, morphology, and wetting properties of *Pseudomonas fluorescens* AR 11 biofilms is assessed. A relationship between flow conditions and biofilm growth and morphology is observed and the role of mass transfer resistance in the fluid on the observed differences is analysed. Pseudomonas biofilms have always shown an amphiphilic wetting behavior independently from the specific culture conditions here investigated.

This work, despite being still a preliminary investigation of a wide and still not understood problem, provides useful information for the analysis of biofilm formation under flow. A detailed knowledge of the relation of biofilm morphology with flow conditions, coupled with information about biofilm interaction with an external phase, as measurable by wetting properties, can provide important support to the design of industrial flow apparatus, where biofilm formation or removal is a relevant (positive or negative) aspect.

CRediT authorship contribution statement

Federica Recupido: Data curation, Formal analysis, Investigation, Methodology, Software, Visualization, Writing - original draft. **Giuseppe Toscano:** Data curation, Formal analysis, Investigation, Methodology, Resources, Validation, Writing - original draft. **Rosarita Tatè:** Data curation, Investigation, Methodology, Resources, Visualization. **Maria Petala:** Project administration, Validation, Writing - review & editing. **Sergio Caserta:** Conceptualization, Formal analysis, Project administration, Software, Supervision, Validation, Writing - original draft, Writing - review & editing. **Thodoris D. Karapantsios:** Conceptualization, Funding acquisition, Project administration, Supervision, Writing - review & editing. **Stefano Guido:** Conceptualization, Funding acquisition, Project administration, Resources, Supervision, Writing - review & editing.

Declaration of Competing Interest

The authors declare that there are no conflicts of interest.

Acknowledgments

Part of this study was funded by Marie-Curie ITN, "*Complex Wetting Phenomena*", *Cowet* (PF7-People 2013-ITN-Grant Agreement N_o 607861). This study was conducted under the umbrella of the European Space Agency Topical Team: Biofilms from an interdisciplinary perspective. This study was conducted under the umbrella of the European Space Agency Topical Team: Biofilms from an interdisciplinary perspective. The authors are thankful to Mrs. Daisy Villano for her support and collaboration to the project and Prof. Giovanni Ianniruberto for his helpful suggestions about transport phenomena correlations.

Appendix A. Supplementary data

Supplementary material related to this article can be found, in the online version, at doi:https://doi.org/10.1016/j.colsurfb.2020.111047.

References

[1] L. Hall-Stoodley, J.W. Costerton, P. Stoodley, Nat. Rev. Microbiol. 2 (2004) 95–108.
[2] H.C. Flemming, J. Wingender, Nat. Rev. Microbiol. 8 (2010) 623–633.
[3] J.W. Costerton, P.S. Stewart, E.P. Greenberg, Science 284 (1999) 1318–1322.
[4] J. Nett, Lincoln, L. Marchillo, K.R. Massey, K. Holoyda, B. Hoff, M. Van Handel, D. Andes, Antimicrob. Agents Chemother. 51 (2007) 510–520.
[5] D. de Beer, A. Schramm, Water Sci. Technol. 39 (1999) 173–178.
[6] R. Van Houdt, C.W. Michiels, J. Appl. Microbiol. 109 (2010) 1117–1131.
[7] K. Drescher, Y. Shen, B.L. Basser, H.A. Stone, Proc. Natl. Acad. Sci. 11 (2013) 4345–4350.

[8] S. Rajbir, P. Debarati, K.J. Rakesh, Trends Microbiol. 9 (2006) 389–397.
[9] L. Feng, Z. Wu, X. Yu, J. Environ. Biol. 34 (2013) 437–444.
[10] B. Halan, K. Bühler, A. Schmid, Trends Biotechnol. 30 (2012) 453–465.
[11] Z.W. Wang, S. Chen, Appl. Microbiol. Biotechnol. 83 (2009) 1–18.
[12] T.R. Garret, M. Bhakoo, Z. Zhang, Prog. Nat. Sci. 18 (2008) 1049–1056.
[13] P. Stoodley, I. Dodds, J.D. Boyle, H.M. Lappin-Scott, J. Appl. Microbiol. 85 (1999) 19–28.
[14] P. Stoodley, Z. Lewandowski, J.D. Boyle, H.M. Lappin-Scott, Biotechnol. Bioeng. 65 (1999) 83–92.
[15] S. Wasche, H. Horn, D.C. Hempel, Water Res. 36 (2002) 4775–4784.
[16] Y. Liu, Hwa Tay J, Water Res. 36 (2002) 1653–1665.
[17] M.K. Kim, F. Ingremeau, A. Zhao, B.L. Basser, H.A. Stone, Nat. Microbiol. 1 (2016).
[18] J. Azeredo, N.F. Azevedo, R. Briandet, N. Cerca, T. Coenye, A. Rita Costa, M. Desvaux, G. Di Bonaventura, M. Hébraud, Z. Jaglic, M. Kaániová, S. Knøchel, A. Lourenço, F. Mergulhão, R.L. Meyer, G. Nychas, M. Simões, C. Sternberg, Crit. Rev. Microbiol. 43 (2017) 313–351.
[19] D.P. Bakker, A. van der Mats, G.J. Verkerke, H.J. Busscher, H.C. van der Mei, Appl. Environ. Microbiol. 69 (2003) 6280–6287.
[20] C. Sternberg, T. Tolker Nielsen, Curr. Protocol Microbiol. 1 (2006) 2–15.
[21] J.S. Teodósio, M. Simões, L.F. Melo, F.J. Mergulhão, Biofouling 27 (2011) 1–11.
[22] W. Zhang, T.S. Sileika, C. Chen, Y. Liu, J. Lee, A.I. Packman, Biotechnol. Bioeng. 108 (2011) 2571–2582.
[23] W. Zhang, T.S. Sileika, A.I. Packman, FEMS Microbiol. 84 (2013) 344–354.
[24] R. Oliveria, L. Melo, A. Olivieria, R. Salguerio, Colloids Surf. B: Biointerfaces 2 (1994) 41–46.
[25] A.K. Epstein, B. Pokroy, A. Seminara, J. Aizenberg, Proc. Natl. Acad. Sci. U. S. A 108 (2011) 995–1000.
[26] M. Werb, C. Falcón García, N.C. Bach, S. Grumbein, S.A. Sieber, M. Optiz, O. Lieleg, Biofilms Microb. (2017) 3–11.
[27] C. Falcón García, F. Stangl, A. Gotz, W. Zhao, S.A. Sieber, M. Optiz, O. Lieleg, Biomater. Sci. 7 (2019) 220–232.
[28] Leibniz Institut DSMZ-Deutsche Sammlung von Mikroorganismen und Zellkulturen GmbH; Curators of the DSMZ, (2020), p. 4348 https://www.dsmz.de/collection/catalogue/details/culture/DSM-4358).
[29] R.B. Bird, W.E. Stewart, E.N. Lightfoot, Transport Phenomena, John Wiley & Sons, Hoboken, New Jersey (USA), 2002.
[30] W.J. Stubbings, J.M. Bostock, E. Ingham, I. Chopra, J. Antimicrob. Chemother. 54 (2004) 139–143.
[31] G.D. Christensen, W.A. Simpson, J.J. Younger, L.M. Baddour, F.F. Barrett, D.M. Melton, E.H. Beachey, J. Clin. Microbiol. 22 (1985) 996–1006.
[32] T.L. Luo, M.C. Eisenberg, M.A.L. Hayashi, C. Gonzalez-Cabezas, B. Foxman, C. Marrs, A.H. Rickard, Nat. Sci. Rep. 8 (2018) 1–14.
[33] A. Heydorn, A.T. Nielsen, M. Hentzer, C. Sternberg, M. Givskov, B.K. Ersbøll, S. Molin, Microbiology 146 (2000) 2395–2407.
[34] M. Vorregaard, Comstat2, A Modern 3D Image Analysis Environment for Biofilms, in Informatics and Mathematical Modelling, Technical University of Denmark, Kongens Lyngby, Denmark, 2008.
[35] B.E. Rittmann, Biotechnol. Bioeng. 24 (1982) 501–506.
[36] J. Kim, H.S. Kim, S. Han, J.Y. Lee, J.E. Oh, S. Chung, H.D. Park, Lab Chip 13 (2013) 1846–1849.
[37] J. Yang, J. McGuire, E. Kolbe, J. Food Prot. 54 (1991) 879–884.
[38] I. Ríos-López, S. Evgenidis, M. Kostoglou, X. Zabulis, T.D. Karapantsios, Colloids Surf. A Physicochem. Eng. Asp. 549 (2018) 164–173.
[39] H.C. van der Mei, R. Bos, H.J. Busscher, Colloids Surf. B Biointerfaces 11 (1998) 213–221.
[40] S.P. Sutera, R. Skalak, Annu. Rev. Fluid Mech. 25 (1993) 1–19.
[41] S.P. Stewart, Biofouling 28 (2012) 187–198.
[42] E.L. Cussler, Diffusion Mass Transfer in Fluid Systems, Cambridge University Press, Cambridge, 1997.
[43] P. Thomen, J. Robert, A. Manmeyran, A.F. Bitbol, C. Douarche, N. Henry, PLoS One 12 (2017) 175–197.
[44] E. Paramonova, O.J. Kalmykowa, H.C. van der Mei, H.J. Brusscher, P.K. Sharma, J. Dent. Res. 88 (2009) 922–936.
[45] H. Rath, S.N. Stumpp, M. Stiesch, PLoS One 12 (2017) 1–12.
[46] K. Welch, Y. Cai, M. Strømme, J. Funct. Biomater. 3 (2012) 418–431.
[47] W.M. Weaver, V. Milisavljevic, J.F. Miller, D.Di Carlo, Appl. Environ. Microbiol. 16 (2012) 5890–5896.
[48] M. Brading, J. Boyle, H.M. Lappin-Scott, J. Ind. Microbiol. 15 (1995) 297–304.
[49] M. Simões, M.O. Pereira, S. Sillankorva, J. Azaredo, M.J. Vieira, Biofouling 23 (2007) 249–258.
[50] P.A. Araújo, J. Malheiro, I. MacHado, F. Mergulhão, L. Melo, M. Simões, J. Environ. Eng. 142 (2016) 1–7.
[51] A.P. Rühs, L. Bocker, G.G. Fuller, R.F. Inglis, P. Fisher, Colloids Surf. B Biointerfaces 117 (2014) 174–184.
[52] V. Carniello, B.W. Peterson, H.C. van der Mei, H.J. Busscher, Adv. Colloid Interface Sci. 261 (2018) 1–14.